Bartenstein, J. E., Liu, X., Lange, K., Claesson, P. M., & Briscoe, W. H. (2018). Polymersomes at the solid-liquid interface: Dynamic morphological transformation and lubrication. *Journal of Colloid and Interface Science*, *512*, 260-271. https://doi.org/10.1016/j.jcis.2017.10.065

Journal of Colloid and Interface Science 512 (2018) 260–271

Contents lists available at ScienceDirect

Journal of Colloid and Interface Science

journal homepage: www.elsevier.com/locate/jcis

Polymersomes at the solid-liquid interface: Dynamic morphological transformation and lubrication

Julia E. Bartenstein [a], Xiaoyan Liu [b], Kathrin Lange [a], Per M. Claesson [b], Wuge H. Briscoe [a,*]

[a] School of Chemistry, University of Bristol, Cantock's Close, Bristol BS8 1TS, UK
[b] Surface and Corrosion Science, Drottning Kristinas Väg 51, Royal Institute of Technology, SE-100 44 Stockholm, Sweden

GRAPHICAL ABSTRACT

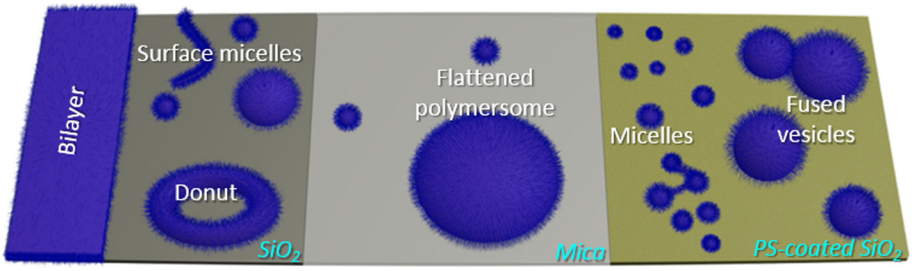

ARTICLE INFO

Article history:
Received 8 June 2017
Revised 13 October 2017
Accepted 16 October 2017
Available online 17 October 2017

Keywords:
Polymersomes
Polymer vesicles
Adsorption
Solid-liquid interface
Self-assembly
Block-copolymers
Lubrication

ABSTRACT

Polymersomes are hollow spheres self-assembled from amphiphilic block copolymers of certain molecular architecture. Whilst they have been widely studied for biomedical applications, relatively few studies have reported their interfacial properties. In particular, lubrication by polymersomes has not been previously reported. Here, interfacial properties of polymersomes self-assembled from poly (butadiene)-poly(ethylene oxide) (PBD-PEO; molecular weight 10,400 g mol^{-1}) have been studied at both hydrophilic and hydrophobic surfaces. Their morphology at silica and mica surfaces was imaged with quantitative nanomechanical property mapping atomic force microscopy (QNM AFM), and friction and surface forces they mediate under confinement between two surfaces were studied using colloidal probe AFM (CP-AFM). We find that the polymersomes remained intact but adopted flattened conformation once adsorbed to mica, with a relatively low coverage. However, on silica these polymersomes were unstable, rupturing to form donut shaped residues or patchy bilayers. On a silica surface hydrophobized with a 19 nm polystyrene (PS) film, the polymer vesicles formed a more stable layer with a higher surface coverage as compared to the hydrophilic surface, and the interfacial structure also evolved over time. Moreover, friction was greatly reduced on hydrophobized silica surfaces in the presence of polymersomes, suggesting their potential as effective aqueous lubricants.

1. Introduction

Polymersomes (or polymer vesicles) self-assembled from block copolymers have been widely studied for a range of biomedical applications [1]. Their formation is driven by the balance between the hydrophobic attraction and the elastic bending energy cost, which is readily facilitated by amphiphilic block copolymers with a hydrophobic to hydrophilic segmental ratio of 35 (± 10)% [2,3], giving rise to polymersomes with diameters usually ranging between ~50 nm and a couple of microns. Because of their structural resemblance with biological cells, i.e. with a bilayer membrane enclosing an inner sac, the vesicles could be used as artificial cell compartments [4] for encapsulation in either the hydrophilic core

* Corresponding author.
E-mail address: wuge.briscoe@bristol.ac.uk (W.H. Briscoe).

https://doi.org/10.1016/j.jcis.2017.10.065
0021-9797/

or the hydrophobic membrane, making them a versatile and promising choice as drug delivery hosts in medical applications [1,5–7]. Furthermore, by incorporating functional groups responsive to external stimuli, the release of an encapsulated drug molecule can be triggered under certain conditions, for example, by varying pH [8,9], temperature [10], or upon hydrolysis [6,11].

Whilst polymer vesicles in bulk solution are widely studied, their behaviour at interfaces is not well understood. In a number of studies, atomic force microscopy (AFM) has been used (sometimes as a complementary technique to other characterisation methods, e.g. cryo-transmission electron microscopy (cryo-TEM) [12]) to image surface adsorbed polymersomes. For instance, polymersomes were adsorbed from dispersions onto a silicon surface and dried either in air [13] or under vacuum [14] before they were imaged. The dried surface polymersomes were found intact but flattened, and drying did not seem to alter the membrane thickness [14]. Imaging polymer vesicles at the solid-liquid interface is more demanding as the polymersomes could be mobile under the scanning tip. To enhance the surface anchorage of the polymersomes, Mg^{2+} bridges were used to bind pluronic polymersomes to mica [15]. It has also been shown using AFM and quartz-crystal microbalance (QCM-D) that intact polymersomes could be incorporated into polyelectrolyte multilayers electrostatically to build up layer-by-layer assemblies consisting of alternating polyelectrolyte and polymersome sheets [16]. Cryo-TEM and AFM analyses of poly-(dimethylsiloxane)-*block*-poly(2-methyloxazoline) (PDMS-*b*-PMOXA) polymersomes deposited on silica and mica showed that, while the polymersomes on silica adopted a stable cap-like conformation, they would fuse on mica and form patchy bilayers [17]. This points to the importance of substrate surface chemistry in the stability and morphology of interfacial polymersomes.

Poly(butadiene)-poly(ethylene glycol) (PBD-PEO) polymersomes have been intensively studied in the past [18–21], and their mechanical properties [22] and *in vitro* compatibility [23] have been closely examined. Using AFM imaging, Li and Palmer [24] have studied PBD-PEO micelles (PBD_{407}-PEO_{286}), worms (PBD_{96}-PEO_{52}) and polymersomes (PBD_{219}-PEO_{121} and PBD_{407}-PEO_{286}) on mica and glass surfaces, showing that substrate chemistry, aggregate geometry, and polymer molecular weight (MW) all influenced interfacial adsorption behaviour. For example, the observed size of surface adsorbed PBD_{407}-PEO_{286} polymersomes (bulk size ~ 70 nm) was nonuniform on mica, in contrast to the PBD_{219}-PEO_{121} polymersomes, which was attributed to weaker interactions with the substrate due to its longer hydrophilic chain length, and thus a higher surface mobility under the scanning AFM tip.

In general, the reports on the interfacial behaviour of polymersomes are limited; in particular, it is little explored how polymersomes might mediate lubrication and surface forces as a model nanofluid [25]. In this study, we have investigated the stability and morphology of PBD_{125}-PEO_{80} [21] polymersomes exposed to hydrophilic and hydrophobic substrates using quantitative nanomechanical property mapping atomic force microscopy (QNM AFM). Our results show a range of surface morphologies due to deformation or rupture of the polymersomes depending on the substrate charge density and hydrophobicity. Measurements of normal and frictional forces complemented the QNM results and gave further insights into adsorption and aqueous boundary lubrication behaviour [26] of polymer vesicles.

2. Experimental methods and materials

2.1. Chemicals

PBD_{125}-PEO_{80}, diblock copolymer (MW = 10,400 g mol^{-1}, PDI = 1.04) was purchased from Polymer Source (Canada). Phosphate buffered saline (PBS) with a physiological pH of 7.4 was purchased from Sigma (Dulbecco's PBS) and polystyrene (MW = 100 kg mol^{-1}) was obtained from Fischer (UK). MilliQ water with a resistivity of 18.2 MΩ cm and a total organic content (ToC) ~ 3 ppb was used throughout. All samples were prepared under ambient condition. The choice of the two solvents, H_2O and PBS represented the two extreme cases of the ionic strength, with PBS a physiological buffer with osmolarity and ion concentrations similar to that of the fluid inside human cells, which is often used in the study of drug delivery applications. We have also previously studied the PBD-PEO polymersome stability in these two solvents [21].

2.2. Sample preparation

PBD_{125}-PEO_{80} polymersomes were prepared *via* a procedure as described in Ref. [21,27]. Briefly, 0.05 g copolymer was dissolved in 4 mL of chloroform in a glass vial. The chloroform was then evaporated under reduced pressure using a vacuum evaporator to form a thin film of polymer on the sides of the vial. Then 4.95 g of H_2O or PBS was added and the mixture stirred at room temperature for 18 h until a cloudy dispersion was formed. The solution was then sonicated for 15 min before it was passed through a lipid extruder to separate different sized polymersomes and other polymer assemblies.

For extrusion, polycarbonate filter membranes of 100 nm or 400 nm pore sizes obtained from Avanti Polar Lipids (USA) were used with a lipid extruder (Avanti® Mini-Extruder). To prepare 400 nm sized polymersomes, the dispersion was passed through a 400 nm membrane in the extruder 41 times. For smaller polymersome sizes, this was further passed through a 100 nm membrane 41 times. The final dispersions were analysed using dynamic light scattering (DLS; Malvern Zetasizer Nano ZS, Malvern Instruments, UK) at 25 °C, and the diameters were found to be 220 nm (PDI 0.10) and 350 nm (PDI 0.10) for polymersomes prepared in H_2O, and 220 nm (PDI 0.13) and 360 nm (PDI 0.15) for polymersomes in PBS for extrusion, using the 100 nm and 400 nm membranes respectively. Note that the PDI values were obtained from DLS, defined as $(s/D_a)^2$ where s is the standard deviation and D_a the mean value of the number averaged polymersome diameter.

Polymer vesicles were studied on hydrophilic silica and mica, as well as hydrophobic polystyrene-coated silica. Silicon wafers were purchased from University Wafer (USA) and was cut into 1 × 1 cm squares using a diamond cutter. The silica substrates were cleaned via sonication for 15 min in ethanol, before rinsing with more ethanol and drying with N_2.

Mica was purchased from S&J Trading (NYC, A1 special grade) from which mica sheets were cleaved in a laminar flow hood and then cut into size (1 × 1 cm) using scissors. Freshly cleaved mica sheets were used for all measurements.

To coat silica with polystyrene (PS), first PS was dissolved in toluene at a concentration of 0.5 mg mL^{-1}. Then 0.2 mL of the PS toluene solution was spin cast onto a UV-Ozone (Jelight 42-200, Jelight Company Inc., USA) cleaned silica wafer (1 × 1 cm) at 500 rpm for 3 s using a spin coater (WS-650MZ-23NPP, Laurell Technologies Corporation, USA), before being spin cast at 3500 rpm over 30 s. This gave 18–20 nm PS nanofilms on silica, as verified by ellipsometry (M-2000 ellipsometer, J.A. Woollam Company Inc., USA) and the RMS surface roughness was determined by AFM to be ~2 nm. The water contact angle on the PS-coated silica was 99.9 ± 1.2° (from 4 measurements), with an example contact angle image shown in Fig. S2 in the Electronic Supplementary Information (ESI) Section.

2.3. PeakForce QNM measurements and imaging

An atomic force microscope (AFM; Nanoscope Multimode 8, Bruker, USA) was used to image surface topography and to study

local surface deformation of adsorbed surface aggregates operating in the PeakForce Tapping mode on hydrophilic silica and mica as well as hydrophobic PS-coated silica. For these measurements, triangular silicon nitride cantilevers with a tip radius of ~2 nm (Scanasyst-Fluid+, Bruker) were used. The PeakForce tapping mode allows imaging at a controlled low feedback force while simultaneously collecting information about the surface material properties [28–30], particularly useful when imaging soft samples such as a hydrated polymer layer in this study. The cantilever spring constant was calibrated by using a method based on thermal noise with hydrodynamic damping of the cantilever [31].

The above PeakForce QNM experiments were carried out in a fused silica liquid cell. First, H_2O or buffer solution was injected into the cell, then the polymersome solution was injected and incubated for one hour. The cell was then rinsed with solvent and the adsorbed polymersome layer imaged. For overnight measurements, the polymersome solution was re-injected after imaging and allowed to adsorb overnight, before the adsorbed layer was rinsed with solvent and then imaged. For all measurements, a peak force of 300 pN and a scan rate of 1 Hz were used. The surfaces were imaged using scan size of 500 nm for individual polymersomes and 1–15 μm for the topography on a larger scale. Typically, measurements were taken at 3 or more different spots, and the images shown in the results section represent example results from a total of at least 6 images taken in each case.

Force curves on bare silica, at the edge of vesicles, and on top of vesicles were performed on single polymersomes, with a setpoint of 1 nN. The force curves were saved by High Speed Data Capture (Hsdc) when imaging, which allows precisely pinpointing the position of the force curve on the image. The forces were measured on at least two different spots, and on each spot more than 15 force curves on both approach and separation of the surfaces were captured, with 10 example forces (5 on approach and 5 on separation respectively) reported in Figs. 9 and 10.

The NanoScope Analysis Version 1.5 (Bruker) software was used to analyse the recorded images and forces. The height images were flattened to remove tilt prior to image analysis. The forces were analysed using the QNM Hsdc Force Curve-Image function.

2.4. Colloidal probe atomic force microscopy (CP-AFM)

Colloidal probe AFM friction measurements were performed using a Bruker Multimode V AFM (USA) coupled with a Nanoscope V controller using procedures described previously [32–34]. 10 μm silica particles (Microparticle GmbH, Germany) were glued using a thermoresponsive 3-component epoxy resin made of dodecenyl succinic anhydride, araldite resin CY 212 and *N*-benzyldimethylamine from Agar scientific (UK) onto tipless cantilevers (CSC38/tipless/Cr-Au, MikroMasch, USA) with lateral spring constants k_{normal} of 0.058 N m^{-1} and 0.057 N m^{-1} and torsional spring constants $k_{torsional}$ of 1.74×10^{-9} Nm rad^{-1} and 1.46×10^{-9} Nm rad^{-1}, respectively. As described previously [32–34], normal force measurements were made on at least 3 different contact spots for each sample, with at least 15 normal force curves were collected at each contact spot. Similarly, each friction force data point at a particular normal force (load) was obtained by averaging over at least 15 trace and 15 retrace scans with a scan size of 5 μm at 1 Hz (thus 10 μm s^{-1}).

2.5. QCM-D

QCM-D measurements were performed using a Q-sense E4 microbalance (Biolin Scientific, Sweden). The resonance frequency f and the energy dissipation D of the crystal can be accurately determined as described by Rodahl et al. [35] In order to convert the measured quantities to a mass, a model has to be invoked [36–38]. The Sauerbrey model [36] assumes that the frequency change only depends on the mass attached to the crystal (Γ_{QCM-D}) as described by the expression

$$\Gamma_{QCM-D} = \frac{-C\Delta f}{n} \tag{1}$$

where n the overtone number, Δf the frequency change, and C a constant specific for the QCM-D crystal type used. In our case, C = 0.177 mg m^{-2} Hz^{-1}. The Voigt model [35] relates the frequency change and the dissipation change to the viscoelastic properties of the adsorbed film, which allows for determination of the adsorbed layer thickness.

The adsorption of the polymersomes was measured at 23 °C at a flow rate of 50 μL min^{-1} in all the QCM-D experiments. Firstly, H_2O or buffer solution was injected into the QCM-D chamber to obtain a stable baseline. Next, the polymersome solution was injected, and after 1.5 h (H_2O) or 24 h (PBS) of adsorption time, the QCM-D chamber was rinsed with the solvent to remove weakly adsorbed polymersomes.

3. Results and discussion

3.1. AFM imaging of PBD-PEO polymersomes

AFM imaging was performed on hydrophilic and hydrophobic surfaces exposed to PBD_{125}-PEO_{80} polymersome dispersions. For silica exposed to 220 nm PBD-PEO polymersomes in H_2O, imaging shows no adsorption of intact polymersomes, but instead a polymer layer with a root mean square (RMS) roughness of 0.5 nm (Fig. 1a). It is assumed that in the polymer bilayer PEO chains were in contact with both silica and also the polymer-water interface, shielding the hydrophobic PBD segments. This polymer layer adsorption was further confirmed by QCM-D measurements as shown in Fig. 1b. Here, the polymersome dispersion was exposed to a quartz crystal and the frequency change due to aqueous polymersome adsorption was found to be below 20 Hz with a dissipation change of around 2×10^{-6}. This suggests limited adsorption of a thin layer with a thickness of around 2 nm as estimated from the Voigt model.

Deformation and rupture of lipid vesicles bound to a surface is a result of the balance between their elastic deformation and adhesion energies and has, for lipid vesicles, been calculated by Seifert and Lipowsky [39] by minimizing the free energy functional F

$$\begin{aligned} F &= F_K + F_W + F_P + F_\Sigma \\ &= \left(\frac{\kappa}{2}\right) \oint dA(C_1 + C_2 - C_0)^2 + \kappa_G \oint dAK - WA^* + P \int dV \\ &\quad + \Sigma \oint dA, \end{aligned} \tag{2}$$

where F_K is the Helfrich curvature of energy [40], which is dependent on the two principal curvatures C_1 and C_2, the spontaneous curvature C_0 and the bending rigidity κ (which for PBD_{125}-PEO_{80} polymersomes has been calculated to 466 ± 157 k_BT [41]), F_W the contact energy term due to the contact potential W arising from the interaction between the vesicle and the surface (W is usually between 10^{-4} mJ m^{-2} for weak adhesion and 1 mJ m^{-2} for strong adhesion [42]), and A^* the contact area. F_P and F_Σ are the energies of the volume and area constraints of the vesicle.

The curvature energy F_K is given from Helfrich's as [40]

$$F_K = \left(\frac{\kappa}{2}\right) \oint dA(C_1 + C_2 - C_0)^2 + \kappa_G \oint dAK, \tag{3}$$

where κ_G is the elastic modulus of the Gaussian curvature and K a topological invariant, which is defined as

$$K = 4\pi(1 - g), \tag{4}$$

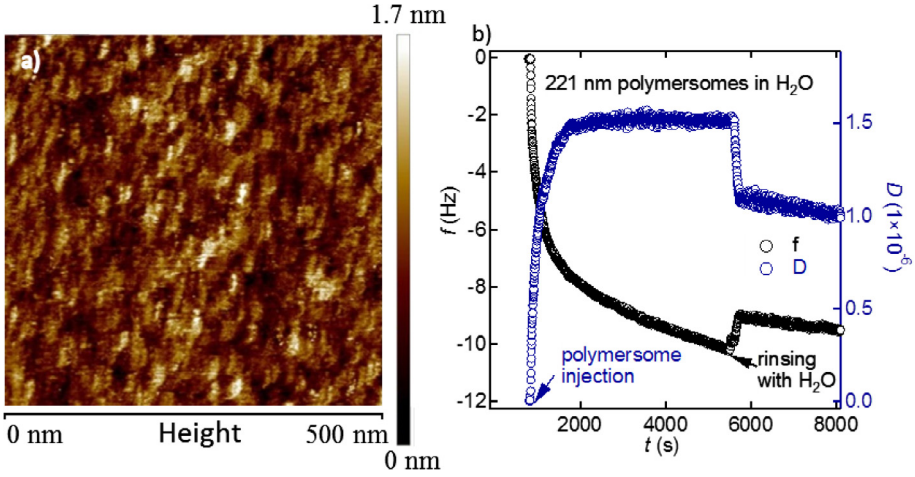

Fig. 1. (a) An example height image of the surface layer on silica adsorbed (~1 h) from an aqueous dispersion of 220 nm PBD-PEO polymersomes; (b) QCM-D frequency change and decay over time for PBD-PEO polymersomes in water.

where g is the genus (number of holes or handles). For a closed vesicle, the topology does not change and K becomes zero; only the first term of in Eq. (3) needs to be considered (thus leading to the first term in Eq. (2).

For large W (i.e. strong vesicle-substrate interactions), Seifert and Lipowsky reported adhesion-induced fusion and rupture of liposomes if the lateral elastic tension Σ due to deformation at the surface experienced by the liposomes exceeded a certain lateral tension Σ_{max}, which is given from the Young-Dupre equation [39]

$$W = \Sigma(1 + \cos\Psi_{eff}), \quad (5)$$

where ψ_{eff} is the effective contact angle between the surface and vesicle. That is, for $W \geq \Sigma_{max}$ the vesicle will rupture and display a disk-like membrane with edge tension Σ_e and energy F_{bd}

$$F_{bd} = -4\pi WR^2 + 4\pi\Sigma_e R \quad (6)$$

where R is the radius of the disk-like membrane after rupture. F_{bd} is always smaller than the energy F_{fd} of a free disk

$$F_{fd} = 4\pi\Sigma_e R \quad (7)$$

However, due to Σ_e the disks will eventually fuse and give rise to a more energetically favourable bilayer [42]. This has also been shown for lipid vesicles at the air-water interface; that is, they rupture and form open lipid disks which would then immediately fuse and form a bilayer [43].

In contrast to the observation in water (cf. Fig. 1a), some polymersomes appeared stable on silica in PBS (1 h incubation time) and remained intact but flattened with sizes in the range of 70–370 nm (mean width 190 nm), with an example image shown in Fig. 2. The sizing of the polymersomes here via the line profile (Fig. 2 inset) was performed on at least 6 images here and for the systems shown in Figs. 4–7 below, with the values and errors shown in Table S1 in the ESI section. Adhesion of vesicles is dependent on R and W [44], and deformation of vesicles bound to a surface is directed by the rigidity κ, which results in a variety of surface adsorbed shapes depending on the change of area A (with its equilibrium value A_0) at constant volume [45]. As the vesicle gains energy during adhesion, its overall energy must be balanced by the cost of curvature energy [42] and the contact, or principal, curvature C of surface bound vesicles can be determined as

$$C = \left(\frac{2W}{\kappa}\right)^{\frac{1}{2}} \quad (8)$$

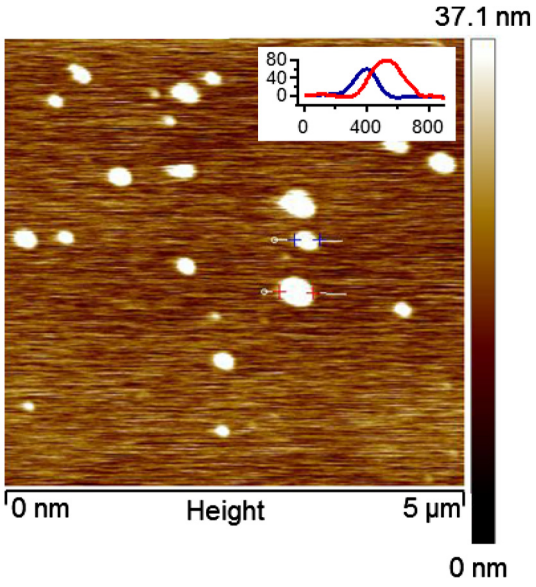

Fig. 2. Example AFM image showing intact 220 nm polymersomes absorbed on silica in PBS (1 h incubation time). The line profiles for two polymersomes are shown in the inset, respectively with a 280 nm base width and 60 nm height (blue) and a 370 nm base width and 78 nm height (red). (For interpretation of the references to colour in this figure legend, the reader is referred to the web version of this article.)

which gives $C \sim 10$ nm^{-1} (strong adhesion) – 1 µm^{-1} (weak adhesion).

In addition to intact PBD-PEO polymersomes shown in Fig. 2, a range of other surface structures with different geometries, e.g. wormlike and donut-shaped aggregates and other fragments, were observed for the same system at a different spot, and example images are shown in Fig. 3. In a cross-sectional analysis of a donut-shaped structure, it appears that the middle of the donut was not flattened, as for example in a red blood cell; instead, the polymersome had rearranged to form a circular structure (Fig. 3c and d). The deformation image (Fig. 3d) shows that the donut appeared more rigid and less deformable than the background. This observation suggests a polymer (bi)layer had adsorbed on the substrate, from fractured polymersomes or free polymer chains in solution, whereas a number of aggregates formed atop of this polymer under layer.

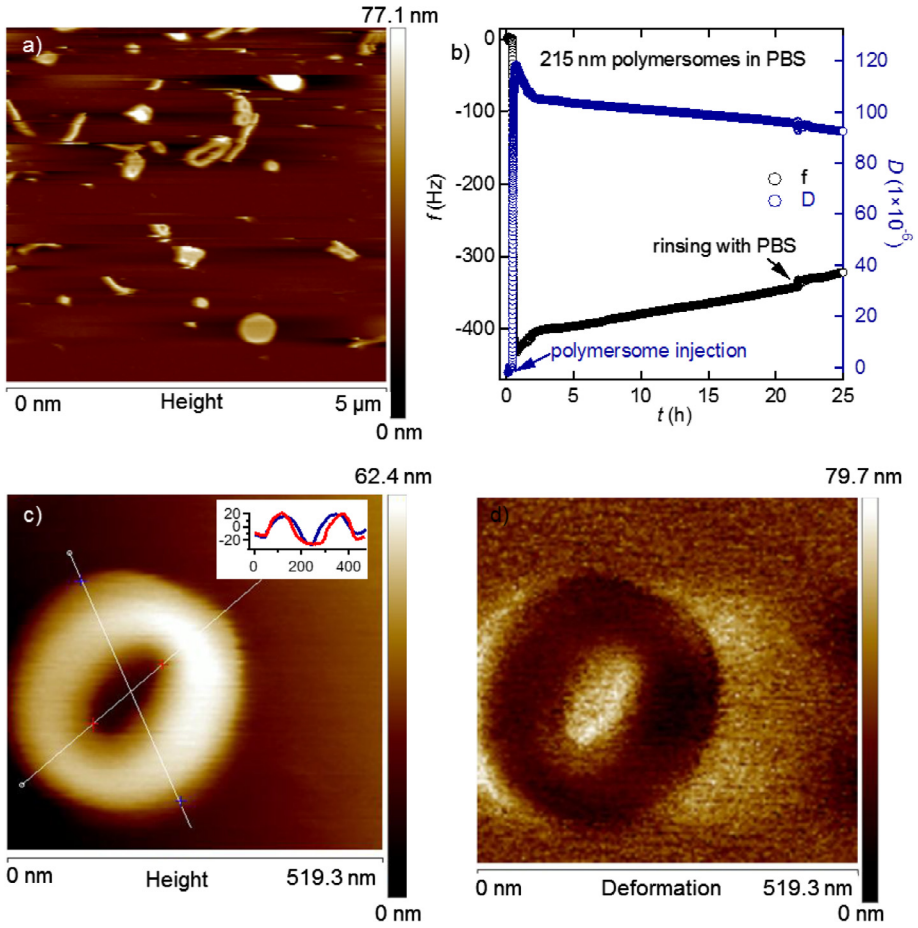

Fig. 3. (a) Example AFM image of silica incubated in 220 nm PBD_{125}-PEO_{80} polymersome PBS dispersions showing ruptured large polymer vesicles giving rise to a range of assemblies, e.g. ring-like and wormlike structures; (b) QCM-D measurements showing the surface structure of polymersomes on a quartz crystal evolved over 24 h, indicating a slow rearrangement towards a bilayer structure; (c) AFM height image of a circular or donut shaped surface aggregate with the line profiles indicating an outer width of 350 nm and height of 22 nm; and (d) AFM deformation image of the same donut aggregate. Compared to the background, the "donut" seemed more rigid, suggesting an underlying polymer bilayer.

To study the effect of adsorption time on the surface aggregate morphology, the silica substrate was incubated in the polymersome dispersion overnight (instead of 1 h), before it was rinsed with water. AFM imaging revealed fewer intact polymersomes as compared with the 1 h incubation time, and, as an example, the height profile of an individual intact polymersome shows that it is more flattened compared to the polymersome after 1 h incubation (Fig. 4). Its diameter was found to be 266 nm with a height of 33 nm. This corresponds to a width-to-height ratio of about 8.1 in agreement with the values reported by Coustet et al. (7.2, for polybenzyl methacrylate-*block*-poly(dimethylamino)ethyl methacrylate polymersomes incorporated into polystyrene sulphonate films on silica) [16] and Battaglia and co-workers (7.8, for poly((2-methacryloyloxy)ethyl phosphorylcholine)-*block*-poly(2-(diisopropylamino)ethyl methacrylate) vesicles immobilized by biotinylated PEG-phospholipid onto silica substrate coated with streptavidin) [46]. The plateau-like conformation indicates surface spreading of the polymersome over time, which could be the early stage of bilayer formation. However, as compared with the system in pure water, the bilayer formation here in PBS seemed slower, which could be attributed to a stabilising effect of the phosphate buffer. In a study from 2001 [47], the stabilising effect of PEG on liposomes in either pure water or buffer solutions was discussed and it was found that PEG-liposomes in PBS were more stable than PEG-liposomes in water. To further test those findings, isothermal titration calorimetry was utilized. The interaction between PEG and phosphate buffers was found to give rise to large endothermic heat flows (–70 cal mol^{-1}), whereas the interaction between PEG and water was slightly exothermic, and that between the phosphate buffer and water was only slightly endothermic. As the effect was only observed with phosphate buffers, it was assumed that the phosphate ions interact with PEG. Furthermore, the presence of phosphate ions inhibited the interactions between PEG-liposomes [47]. In our case, this would suggest that phosphate-PEG binding could compete with interactions between two polymersomes or between polymersomes and a surface adsorbed bilayer, preventing (or slowing down) rupture and resulting in better stabilised polymer aggregates.

AFM imaging of silica exposed to larger 360 nm polymersome PBS dispersions showed similar results (Fig. S1 in the ESI). Complementary QCM-D measurements (Fig. 3b) revealed a frequency change Δf of around 450 Hz upon polymersome adsorption, larger than expected for a polymer layer. It corroborates with the AFM imaging results that intact polymersomes remained on the surface. The QCM-D curve also shows that, after an initial 2.5 h of fast polymersome adsorption, the frequency slowly increased and dissipation decreased over 22 h. This is consistent with a process where the sensed mass decreased slowly due to structural changes towards a thinner layer and a less extended conformation, due to slow spreading of the polymersomes on the surface with time.

Mica was also used as a hydrophilic substrate for adsorption of the 220 nm and 360 nm polymersomes in PBS. AFM imaging

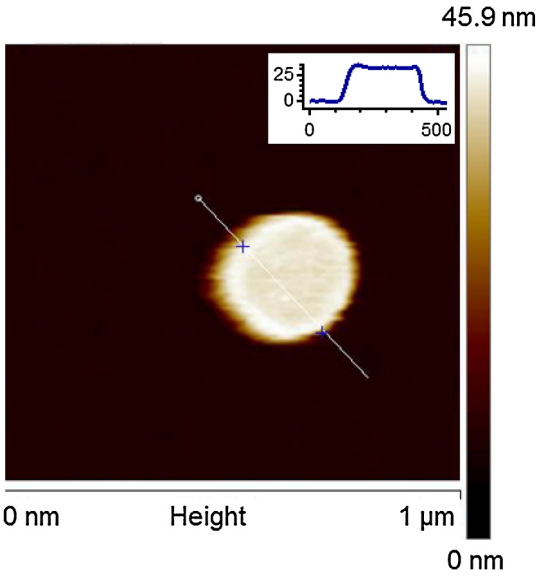

Fig. 4. Example AFM image of an intact 220 nm polymersome on silica in PBS after overnight adsorption with line profile showing a plateaued top with a base diameter of ~266 nm and a height of 33 nm.

revealed low surface coverage (Figs. 5 and 6) of polymersomes, as compared with that on silica (cf. Fig. 3a), ascribable to low affinity of PEO chains to mica. In contrast to adsorption on silica substrates, the 220 nm and 360 nm polymersomes on mica showed different surface characteristics based on their size. For 220 nm polymersomes, presence of smaller fragments of up to 100 nm in diameter and a cap-like adsorption profile (an example shown in Fig. 5b) was observed. The line profile of an individual aggregate showed a base width of 75 nm and a height of 12 nm, giving an aspect ratio of 6.25. In general, the aspect ratio falls in the range of 5.5–14.3. This low surface affinity is assumed to be due to a low contact adhesion energy W of the polymersomes to the mica surface. However, as the adsorbed fragments are rather small, the polymersomes must have ruptured during contact with the surface, which might be due to large curvature energy costs for small vesicles.

For larger (360 nm) polymersome dispersions, surface coverage of the adsorbed aggregates was low, but some polymersomes were observed on mica in PBS (Fig. 6). The height profile in Fig. 6b shows a typical adsorbed structure, with a diameter of 1240 nm and a height of 38 nm, giving a rather large width-to-height ratio of 32.6, which could be due to the polymersome fusing and merging to the surface. The curvature energy cost of a surface deformed vesicle is smaller for a larger polymersome; however, a larger contact area would result in a larger contact potential contribution (the third term in Eq. (2)). In a previous AFM study of PBD_{219}-PEO_{121} (size ~ 70 nm) and PBD_{407}-PEO_{286} (size ~ 50–70 nm) polymersome dispersions in PBS on mica it was found that the vesicles adsorbed in a flattened conformation but remained intact, with a higher surface coverage than that observed here [24]. This study also discussed how a higher polymer molecular weight could result in weaker interactions between mica and the sample, which was ascribed to the longer hydrophilic chains with a smaller affinity to the mica surface. However, the polymersomes we report here were made from a lower molecular weight polymer and as such our observation could not have been explained by the suggested mechanism of adsorption.

To compare with hydrophilic silica and mica, a hydrophobic surface, i.e. 18–20 nm polystyrene (PS)-coated silica, was also used. In water, 220 nm polymer vesicles ruptured, presumably due to hydrophobic interactions between the PBD segments and the PS surface, and formed small islands (40–70 nm in diameter and 1–2 nm height) made of fractured vesicles (Fig. 7a). Here, the contact adhesion W (cf. Eq. (5)) is stronger due to the hydrophobic interactions between PBD chains with PS, compared to the W between PEO and silica or mica, resulting in rupture of the polymersomes at the surface as the maximum lateral surface tension Σ_{max} that the polymersomes could endure is exceeded. Additionally, the curvature of the system was reduced over time while spreading out and forming a bilayer. After 8 h incubation, the small islands were observed to merge (Fig. 7b) and after 18 h, the merged surface aggregates started to spread and thin out over the substrate, forming interconnecting networks (Fig. 7c). It is conceivable that the polymer assemblies were in the process of forming a polymer layer where PBD interacted with PS and the PEO chains shielded the hydrophobic chains from the aqueous solvent. In contrast, larger 360 nm polymersomes appeared more stable (Fig. 8a and b), possibly due to a smaller elastic energy cost than the smaller polymersomes, with some polymersomes merging overnight and forming bigger surface assemblies. As for the 220 nm sized polymersomes, a relatively large contact adhesion W was observed, but as the polymersomes did not rupture, W must

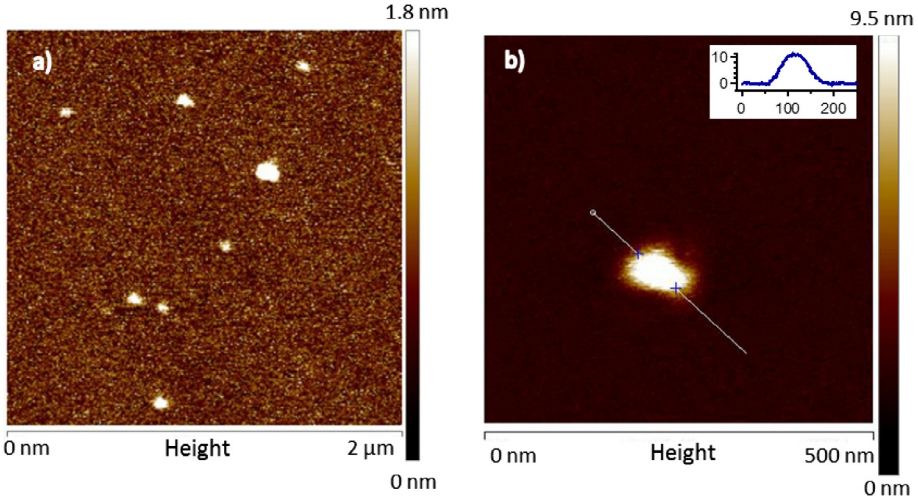

Fig. 5. (a) Example AFM image of 220 nm polymersomes in PBS adsorbed on mica (1 h incubation); (b) Line profile of an individual surface aggregate, showing a flattened conformation with a 12 nm height and a 75 nm base width.

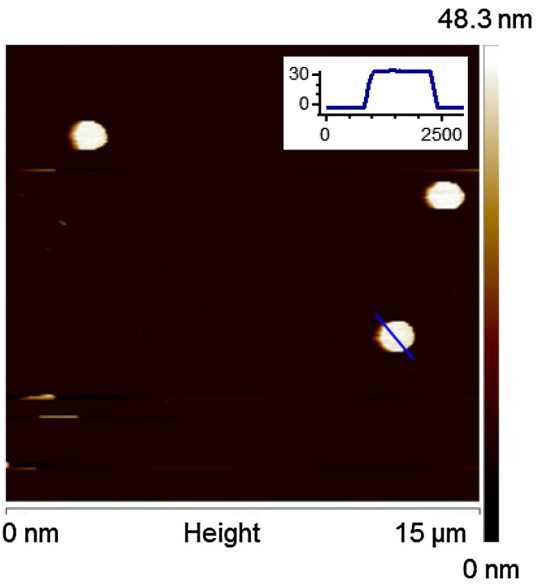

Fig. 6. Example AFM image of 360 nm polymersomes adsorbed on a mica substrate in PBS. The inset shows the cross-sectional profile of an individual polymersome, showing a flattened conformation with 38 nm in height and 1240 nm in base width.

be smaller than Σ_{max}. Eq. (5) shows the dependence of W and Σ_{max} on the contact angle ψ_{eff} between the surface and vesicle. As the contact angle varies with polymersome size due to the size dependent bending energy, the bigger polymersomes initially remain stable on PS-coated substrates, whereas the smaller vesicles rupture. However, some larger surface structures are observed, especially after overnight adsorption, suggesting that vesicles ruptured and fused over time.

In PBS, intact polymersomes were adsorbed onto the hydrophobic surface for both the 220 nm and 360 nm polymersome dispersions, with some inter-vesicle fusion taking place over 24 h. As discussed above, phosphates might bind to the PEO segments, and this would amount to a reduced interaction potential W between the polymersomes with the substrate, suppressing polymersome rupture. This concurs with the observation on the hydrophilic surfaces that PBS stabilised the vesicles. Fig. 8 shows example AFM images for 360 nm polymersomes after 1 h (Fig. 8c) and overnight (Fig. 8d) adsorption in PBS. However, vesicle merging was slower than for the samples in water, which again indicates that PBS was stabilising the polymersomes in solution and on the surface. It was also noted that the surface coverage for PBS samples was higher than in pure water.

In general, for all samples measured, the surface coverage of intact polymersomes and derived aggregates on PS-coated silica was higher than for that on hydrophilic surfaces, which suggests that W (cf. Eq. (2) is stronger between the PBD segments with the PS-coated surfaces than W between PEO-chains and the hydrophilic surface. For larger vesicles in H_2O and aggregates in PBS, W between PBD and PS-coated surfaces was lower and hence some intact polymersomes could be observed even after overnight adsorption. As κ is independent of size, it was assumed that both vesicle sizes in H_2O would rupture; however, the bigger polymersomes were more stable due to a smaller curvature energy penalty.

3.2. Nanomechanical properties of polymersomes at the surface

The nanomechanical properties of an adsorbed individual polymersome were probed by force measurements using a nanotip (of radius ~ 2 nm) with QNM AFM in PBS. To measure force curves, a single intact polymersome or polymersome-like aggregate was focussed upon, and force measurements were made at the edge and on top of the polymersome. Firstly, as a control, normal force curves on bare silica (Fig. 9a), showed no adhesion and no hysteresis upon loading or unloading. At the edge of a 220 nm polymersome, repulsion upon loading and an adhesion of ~1.2 nN upon unloading can be observed (Fig. 9b). In contrast, on top of the polymersomes only a small adhesion (~0.1 nN) was present which might be due to deformation of the hollow central region of the vesicle (Fig. 9c). Both 220 nm and 360 nm polymersomes on silica showed this behaviour. The difference in adhesion at the edge and on top of the polymersome is attributable to the vesicular shape. As the tip approaches the hollow central region of the polymersome, it could deform the polymersome instead of penetrating the membrane. This means that, upon retraction, the tip could be withdrawn without having to get through the polymersome membrane first, which would cause a lower adhesion. At the edge of polymersomes, however, the tip would start to penetrate the polymer layer, which gives rise to a larger adhesive force upon retraction.

On mica on the other hand, the interaction of a bigger 360 nm polymersome with the tip was largely repulsive at the edge and on top of 220 polymersomes and showed only small hysteresis between trace and retrace (Fig. 10). This implies that a different surface structure must have formed on mica, with different polymer packing density and elastic properties. Within a previous study of force measurements on PBD_{407}-PEO_{286} polymersomes on mica [24], a small adhesive jump-in at ~2 nN applied force during trace/compression was observed, which was attributed to the AFM tip breaking through the bilayer membrane of the polymersome. As our vesicles are prepared from lower molecular weight polymers, the membrane thickness will be thinner and the bending rigidity lower; hence the tip can deform the polymersomes more easily without breaking through the membrane.

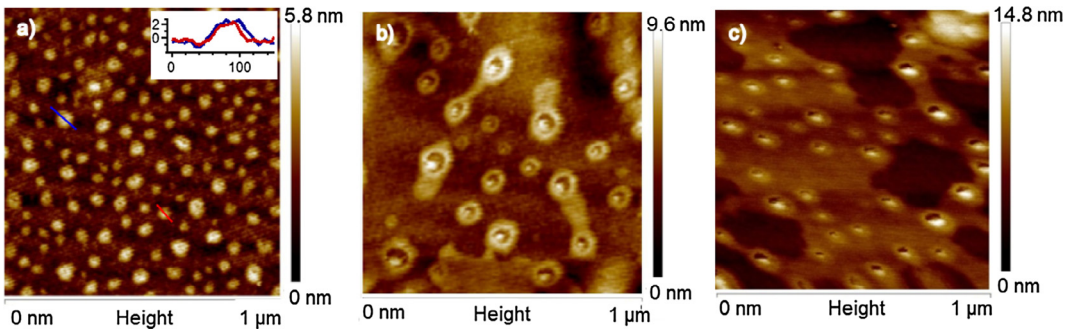

Fig. 7. Example AFM images showing the time evolution of the morphology of the surface layer on hydrophobic PS-coated mica from the 220 nm PBD-PEO polymersome PBS dispersion. (a) After 1 h of incubation, the polymersomes were adsorbed onto the substrate in the form of small islands; (b) after 8 h of incubation, the small islands began to emerge; and (c) after overnight adsorption, the droplets started to fuse, spreading and thinning out, forming a layer of polymer on the substrate.

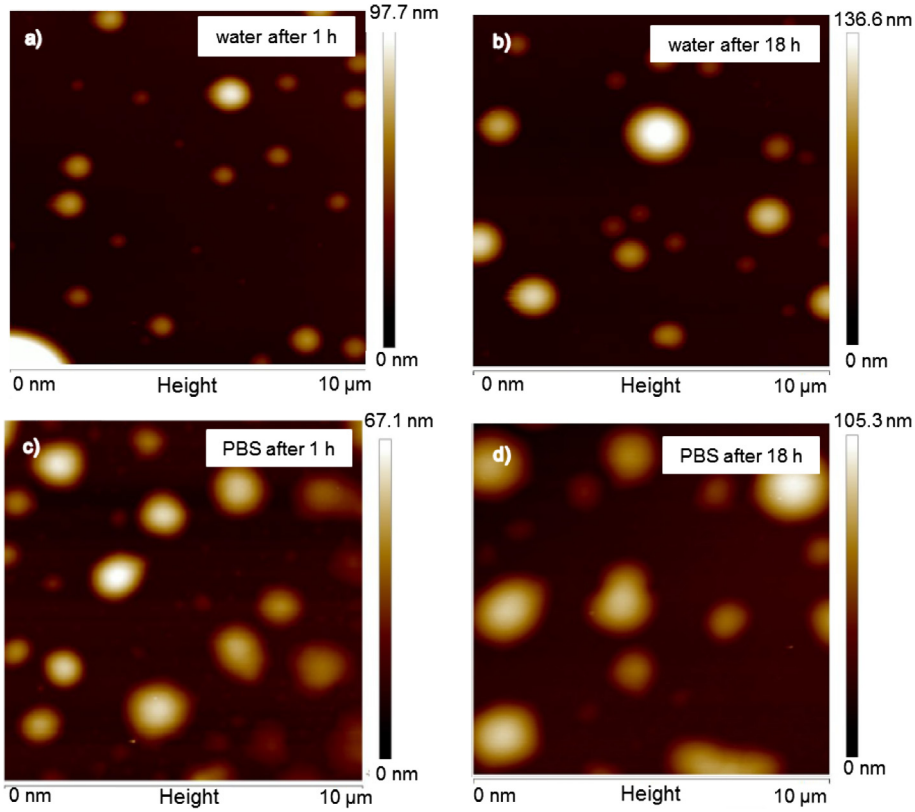

Fig. 8. Example AFM images of surface morphology of PBD-PEO polymer vesicles on hydrophobic PS-coated silica: in polymersome (350 nm) dispersions in water, after 1 h (a) and 18 h (b) incubation; in polymersome (360 nm) PBS dispersions, after 1 h (c) and 18 h (d) incubation.

For polystyrene-coated substrates, interactions between the tip and the hydrophobic surface in water and PBS were attractive. However, after polymersome adsorption, the forces between the tip and a polymersome-like surface aggregate were repulsive upon approach and showed only a very small adhesion upon retrace, indicating similar elastic properties of the surface aggregate to that for samples on mica (Fig. 11). There was little difference between the edge and the centre of the polymersome, suggesting a more uniform polymer packing in the surface aggregates. This is consistent with the picture of the PBD segments in the polymersome merging with the PS surface forming surface assemblies; whereas on hydrophilic surfaces, the polymersome deformed or flattened, retaining a hollow conformation in the centre. As such, the nanomechanical measurements complement our interpretation of the surface structure of the polymersome aggregates observed from AFM imaging.

3.3. Normal forces and friction mediated by polymersomes on the hydrophobic surface

Normal and frictional forces were measured between a 10 µm silica colloidal probe and bare or PS-coated silica using colloidal probe AFM (CP-AFM). Force measurements were conducted first in PBS solution and then in the 360 nm PBD-PEO polymersome PBS dispersion, and representative normal and shear force curves are shown in Fig. 12.

A short ranged repulsive force was observed between silica in the PBS solution (empty red[1] circles in Fig. 12a), attributed to the electrical double layer interaction. Addition of polymersomes to the PBS solution resulted in a longer ranged, soft repulsive force, which is consistent with the adsorption of a polymer layer. Such forces varied in both range and magnitude at different contact spots, indicating that the surface coverage of the polymersomes was inhomogeneous, consistent with AFM imaging (cf. Fig. 3 for 220 nm polymersomes). Two examples of force curves are shown in Fig. 12a (filled and crossed circles) taken at two different contact spots. With the CP-AFM, it is impossible to ascertain the residual surface layer thickness or indeed if the adsorbed polymersome layer was squeezed out, as the zero contact in AFM is determined by a compliant region in the deflection-displacement plot.

On PS-coated silica, the range of the repulsive force again increased upon addition of polymersomes to PBS (empty blue diamonds shifting to filled diamonds in Fig. 12a). The normal force traces obtained here were reproducible in the magnitude and range, which suggests that the coverage of the adsorbed polymer layer was higher and more uniform than on the bare silica substrate. This is in agreement with the corresponding AFM images (cf. Fig. 8), which show that polymersomes adsorbed onto the PS-coated substrate and gave rise to high surface coverage. In comparison to polymersomes on bare Si, the interaction range here is decreased, which indicates that the polymer aggregates adsorbed on PS-coated Si adopted a more compact conformation, possibly due to polymersome deformation or rupture.

As control, friction measurements (Fig. 12b) were carried out in PBS on bare silica surfaces first, both upon increasing load (loading) and decreasing load (unloading) as indicated by the arrows in the figure. The average friction coefficient μ, which can be calculated from the slope of the friction versus load graphs, was ~0.19 ± 0.01 (empty red circles; Fig. 12b). Upon addition of 360 nm polymersomes in PBS, the friction coefficient remains comparable (μ = 0.24 ± 0.01; filled circles), indicating that at such weak

[1] For interpretation of color in Fig. 12, the reader is referred to the web version of this article.

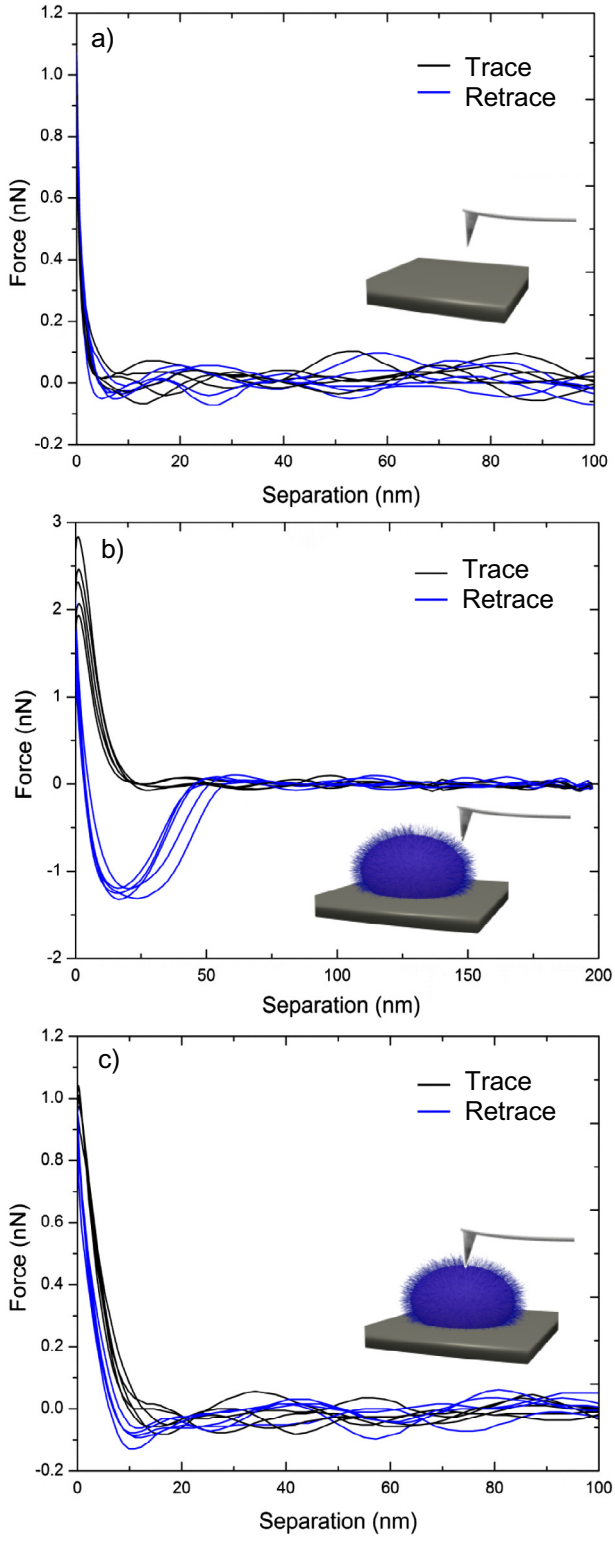

Fig. 9. Force measurements (a) on bare Si; (b) at the edge of, and (c) on top of an individual 220 nm polymersome in PBS.

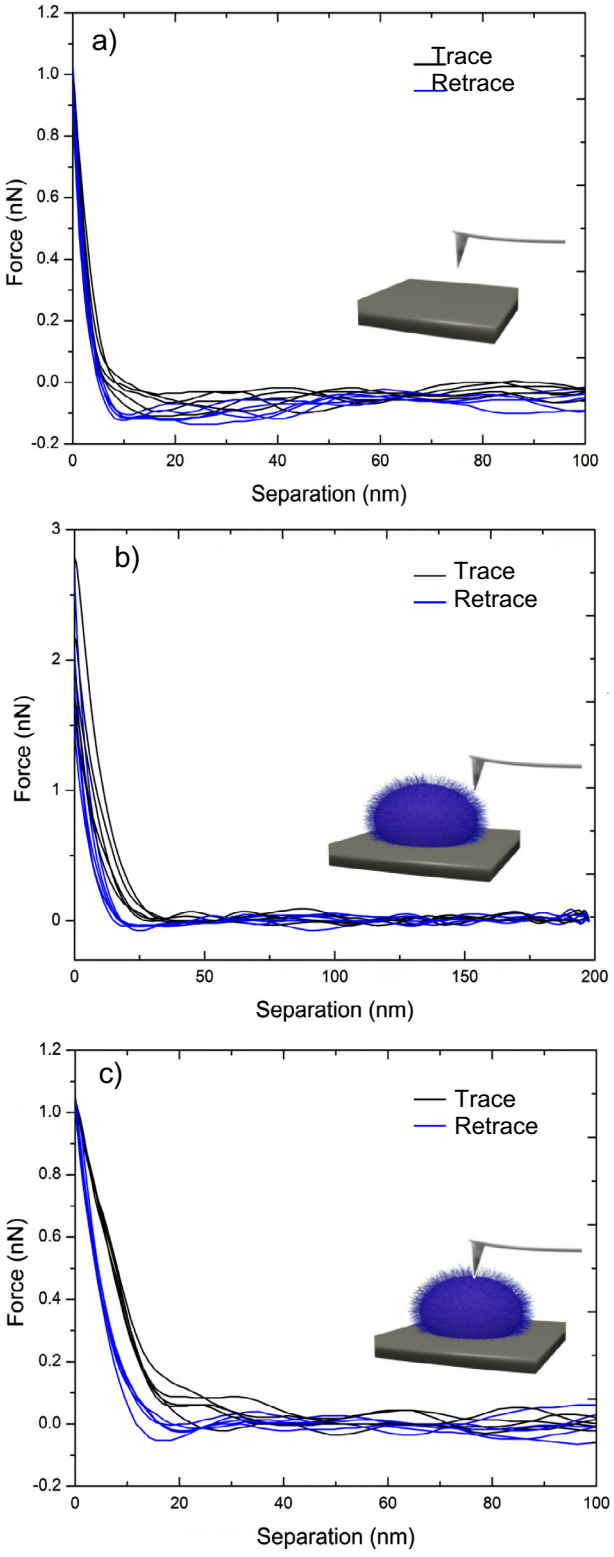

Fig. 10. Force curves recorded on (a) bare mica; (b) at the edge, and (c) on top of a 360 nm polymersome in PBS.

adsorption with low surface coverage did not facilitate effective lubrication. This was true for friction measurements performed at different contact spots. As the polymer vesicles were not very stable under these conditions (cf. Figs. 2 and 3), it is likely that in the friction measurements the colloidal probe glided over or collided with deformed polymersomes or their surface fragments.

The friction versus load curve of the polymersomes showed a linear behaviour above 4 nN with little hysteresis between loading and unloading. It is worth noting that there appears a different regime at low load. In the case when $F < \sim 4$ nN for the friction – load trace shown in Fig. 12(b), the friction coefficient is very low (μ = 0.03 ± 0.01), although the number of data points is limited

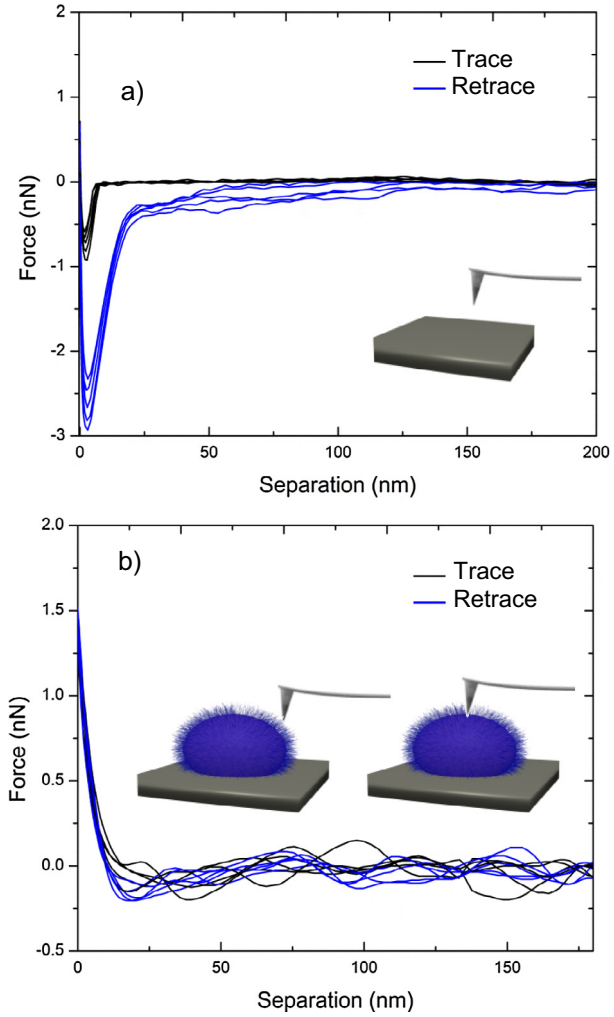

Fig. 11. Force curves recorded on (a) bare PS-coated Si; (b) at the edge and on top of 360 nm polymersomes.

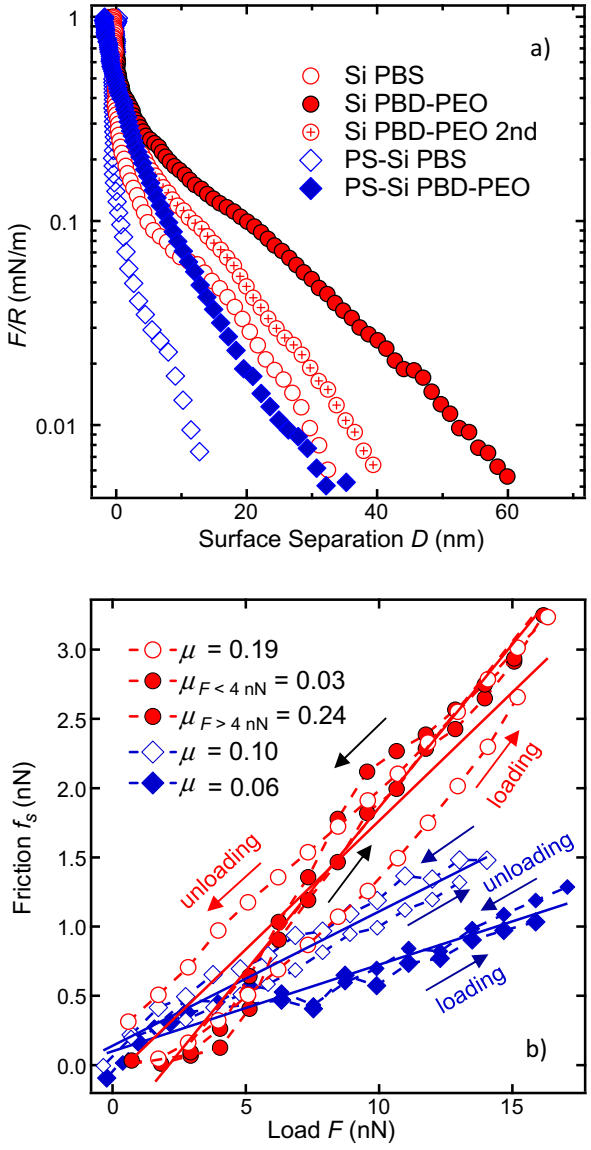

Fig. 12. Normal force (a) and shear force (b) curves obtained on Si and PS-coated Si in PBS and with added 360 nm polymersomes. The symbols in (b) have the same meanings as those in (a), as indicated in the (a) inset. Friction forces measured upon both loading (i.e. increasing the normal force load F) and unloading (i.e. decreasing F) are shown, as indicated by the arrows. Solid lines in (b) are linear fits to both the loading and unloading friction forces for each condition, and thus the slopes of these fits yield the average friction coefficient μ for these systems as given in the inset.

to fully substantiate this regime. We suggest that at the initial contact between the AFM colloidal probe and the adsorbed polymersome layer under such a low load, effective lubrication was mediated between the hydrated polymer layer on the exterior of the polymersomes and the silica colloidal probe. Such low friction is assumed to be based on the hydration lubrication mechanism, which conjectures that lubrication is achieved due to the fluidity of water molecules tenaciously bound in the primary hydration layer of the highly hydrated hydrophilic blocks [48]. Upon load increase, the polymersome was either pushed aside or collapsed, and the hydration lubrication mechanism was no longer operational, leading to a relatively high friction coefficient of 0.24 ± 0.01.

Friction measurements were also performed on PS-coated Si. As control, the friction coefficient μ was found to be around 0.10 ± 0.004 in the PBS solution. Adding polymersomes to the system resulted in a decrease in the friction coefficient to ~0.06 ± 0.005. The corresponding AFM images (Fig. 8) show that adsorbed polymersomes formed a stable layer on the hydrophobic surface with a relatively high surface coverage. It is thus conceivable that polymersomes were flattened or ruptured on the hydrophobic surface, forming a dense layer with the PEO segments pointing outwards, shielding the underlying hydrophobic surface from the aqueous environment. Upon loading and unloading in the friction measurements, the polymer layer remained confined between the probe and the substrate, i.e. it was not squeezed out of the contact zone, thereby facilitating effective lubrication via the hydration lubrication mechanism through the PEO segments. Even though such hydration lubrication has not been observed for polymersomes before, densely packed liposomes, which are structural analogues of polymersomes, were found to remain stable on mica under confinement and give rise to friction coefficients μ as low as 2×10^{-5} [49]. In another study, liposomes were found to rupture upon adsorption on mica and form bilayer stacks, but also provide for low friction coefficients ($\mu \sim 10^{-4}$) [50]. Similarly, low μ were achieved with polymer layers, e.g. poly[2-(methacryloyloxy) ethyl phosphorylcholine] brushes, anchored onto mica [51]. Additionally, electrostatically anchored PEG polymer brushes have been found to provide for comparable low friction ($\mu \sim$ 0.03–0.04) in aqueous media [52]. These studies indicate that PBD-PEO polymersomes, or surface aggregates from these polymersomes, could give

low μ at high surface densities. However, in contrast to the liposome and polymer studies mentioned above, the polymersomes used in this study are not charged. The lubrication of uncharged polymers has, for example, been studied using poly(l-lysine)-poly (ethylene glycol) (PLL-PEG) brushes in 4-(2-hydroxyethyl)pipera zine-1-ethanesulfonic acid buffer (HEPES, adjusted to pH 7.4) using a mini traction machine [53]. In comparison to pure HEPES solution, addition of polymer resulted in a lowering of the friction coefficient, which was thought to be due to the formation of a boundary lubricating film with exposed PEG chains [53]. It is hence assumed that the PEO groups of the PBD-PEO polymersomes would be able to facilitate effective hydration lubrication. The friction over load profile in Fig. 12b furthermore shows an almost linear load dependence, with little hysteresis observed between loading and unloading. These observations suggest that the surface structures from PBD-PEO polymersomes were rather stable, which underpinned the low friction coefficients observed.

4. Summary and concluding remarks

We have studied the interfacial properties of PBD125-PEO80 polymersomes adsorbed at solid/liquid interfaces, and related reports on polymersome interfacial behaviour in the literature are limited. It is shown that the surface coverage and the morphology of the adsorbed polymersomes depended on the polymersome-surface interactions (tuned by using H_2O or PBS, and by varying the substrate surface chemistry), and on the polymersome elastic properties (tuned by using different polymersome sizes). In particular, on the hydrophobic surface we have observed morphological evolution of the adsorbed aggregates due to polymersome fusion on the surface, and a dense surface layer of exposed PEO segments, which facilitated effective hydration lubrication [26]. We expand on these key findings with an outline of the experimental observations below, to highlight the complexity due to the interplay of different parameters.

First, PBD-PEO polymersomes adsorbed on hydrophilic (i.e. silica and mica) and hydrophobic (i.e. PS-coated silica) substrates in either H_2O or PBS solutions were studied using AFM imaging. On silica surfaces, the polymersomes ruptured and showed a tendency towards forming bilayer-like surface structures. Vesicles adsorbed on mica appeared either broken (for smaller 220 nm polymersomes) or merged on the surface (for larger 360 nm polymersomes), with a low surface coverage. These observations on the hydrophilic surfaces are broadly consistent with those reported in a previous AFM imaging study of PBD-PEO polymersomes with different MWs on mica and glass surfaces [24]. However, on more hydrophobic polystyrene-coated silica surfaces, the adsorption morphology was dominated by the favourable hydrophobic interactions between PS and the PBD segments, and importantly, we observed morphological evolution of the adsorbed surface aggregates as a function of time which had not been previously reported. That is, smaller polymersomes ruptured and formed droplet-like polymer assemblies, which merged over time to form networks. Larger polymersomes and polymersomes in PBS adsorbed on the surface without rupturing upon initial adsorption; however, fusion of polymersomes was observed for longer incubation time, indicating that the surface stability of the polymersome was not long term.

Secondly, colloidal AFM friction measurements did not show effective lubrication on silica due to low surface coverage of the adsorbed layer, with the friction coefficient obtained comparable to that obtained in the absence of polymersomes. In contrast, a very low friction coefficient $\sim$0.06 ± 0.005 was observed between the silica colloidal probe and the hydrophobic polystyrene coated silica in the presence of polymersomes. In this case, the polymersome adsorption formed a dense surface layer, exposing the hydrated PEO segments, facilitating hydration lubrication.

Our results on the surface morphologies and stability of adsorbed polymersomes on hydrophilic and hydrophobic substrates, and the lubrication efficiency of the resultant surface structures, are relevant to potential applications where the interfacial properties of polymersomes are an important consideration. In this study, we have compared H_2O or PBS solutions, which represent two rather extreme cases of ionic strength. It paves the way for further investigations by systematically studying the effect of ionic strength and possible ion specificity by using different monovalent and monovalent electrolytes. The polymersome-surface interactions could be further tuned by introducing charges in the hydrophilic segments. Here, we have used colloidal probe AFM to study the frictional properties of an asymmetric system on the hydrophobic surface, i.e. a 10 μm silica particle *vs.* PS. Future work could explore the symmetric PS particle *vs.* PS surface as a more model system, and using nanotextured substrates [32–34] to probe how nanostructures might induce polymersome rupture. In addition, the surface force apparatus (SFA) [51,54] could also be used to yield mechanistic understanding of the frictional behaviour of adsorbed polymers in which a relatively large contact area (compared to AFM) ensures multi-polymersome contact and the absolute surface separation could be determined unequivocally, so that the interactions could be better correlated with the structure of the surface layer. Furthermore, the interfacial structure of the adsorbed polymer layer could also be probed by using synchrotron X-ray reflectivity (XRR) to allow a structure-interaction correlation [55–58].

Acknowledgements

We acknowledge funding from the Engineering and Physical Science Research Council (EPSRC EP/H034862/1), the Royal Society, Taiho Kogyo Tribology Research Foundation (TTRF), the European for Cooperation in Science and Technology (CMST COST) Action CM1101, and the Marie Curie Initial Training Network (MC-ITN) "*Soft, Small, and Smart: Design, Assembly, and Dynamics of Novel Nanoparticles for Novel Industrial Applications (NanoS3)*" (FP7 Grant No. 290251). All underlying data are provided within this paper and as supporting information accompanying this paper.

Appendix A. Supplementary material

Supplementary data associated with this article can be found, in the online version, at https://doi.org/10.1016/j.jcis.2017.10.065.

References

[1] F. Meng, Z. Zhong, J. Feijen, Biomacromol 10 (2009) 197–209.
[2] B.M. Discher, Y.-Y. Won, D.S. Ege, J.C.-M. Lee, F.S. Bates, D.E. Discher, D.A. Hammer, Science 284 (1999) 1143–1146.
[3] H. Aranda-Espinoza, H. Bermudez, F.S. Bates, D.E. Discher, Phys. Rev. Lett. 87 (2001) 208301.
[4] J. Kowal, X. Zhang, I.A. Dinu, C.G. Palivan, W. Meier, ACS Macro Lett. 3 (2013) 59–63.
[5] S. Li, B. Byrne, J. Welsh, A.F. Palmer, Biotechnol. Progr. 23 (2007) 278–285.
[6] F. Ahmed, D.E. Discher, J. Control. Release 96 (2004) 37–53.
[7] Y. Mai, A. Eisenberg, Accounts. Chem. Res. 45 (2012) 1657–1666.
[8] M.S. Kim, D.S. Lee, Chem. Commun. 46 (2010) 4481–4483.
[9] S.W. Kang, Y. Li, J.H. Park, D.S. Lee, Polymer 54 (2013) 102–110.
[10] H. Xu, F. Meng, Z. Zhong, J. Mater. Chem. 19 (2009) 4183–4190.
[11] I.F. Uchegbu, Expert Opin. Drug Del. 3 (2006) 629–640.
[12] R. Gref, Y. Minamitake, M.T. Peracchia, V. Trubetskoy, V. Torchilin, R. Langer, Science 263 (1994) 1600–1603.
[13] A.-L. Brocas, M. Gervais, S. Carlotti, S. Pispas, Polym. Chem.-UK 3 (2012) 2148–2155.
[14] O. Uzun, H. Xu, E. Jeoung, R.J. Thibault, V.M. Rotello, Chem.-A Eur. J. 11 (2005) 6916–6920.
[15] F. Li, T. Ketelaar, M.A. Cohen Stuart, E.J.R. Sudholter, F.A.M. Leermakers, A.T.M. Marcelis, Langmuir 24 (2007) 76–82.

[16] M. Coustet, J. Irigoyen, T.A. Garcia, R.A. Murray, G. Romero, M. Susana Cortizo, W. Knoll, O. Azzaroni, S.E. Moya, J. Colloid Interface Sci. 421 (2014) 132–140.
[17] K. Jaskiewicz, M. Makowski, M. Kappl, K. Landfester, A. Kroeger, Langmuir 28 (2012) 12629–12636.
[18] H. Bermúdez, H. Aranda-Espinoza, D.A. Hammer, D.E. Discher, EPL 64 (2003) 550.
[19] M. Kocun, W. Mueller, M. Maskos, I. Mey, B. Geil, C. Steinem, A. Janshoff, Soft. Matter. 6 (2010) 2508–2516.
[20] Y.-W. Chang, J.A. Silas, V.M. Ugaz, Langmuir 26 (2010) 12132–12139.
[21] J.E. Bartenstein, J. Robertson, G. Battaglia, W.H. Briscoe, Colloid Surf. A 506 (2016) 739–746.
[22] R. Rodriguez-Garcia, M. Mell, I. Lopez-Montero, J. Netzel, T. Hellweg, F. Monroy, Soft Matter 7 (2011) 1532–1542.
[23] J.C.M. Lee, H. Bermudez, B.M. Discher, M.A. Sheehan, Y.-Y. Won, F.S. Bates, D.E. Discher, Biotechnol. Bioeng. 73 (2001) 135–145.
[24] S. Li, A.F. Palmer, Macromolecules 38 (2005) 5686–5698.
[25] G.A. Pilkington, W.H. Briscoe, Adv Colloid Interface 179 (2012) 68–84.
[26] W.H. Briscoe, Curr. Opin. Colloid In 27 (2017) 1–8.
[27] F.M. Menger, M.I. Angelova, Acc. Chem. Res. 31 (1998) 789–797.
[28] F. Rico, C. Su, S. Scheuring, Nano Lett. 11 (2011) 3983–3986.
[29] K. Sweers, K. van der Werf, M. Bennink, V. Subramaniam, Nanoscale Res. Lett. 6 (2011) 270.
[30] M. Sababi, J. Kettle, H. Rautkoski, P.M. Claesson, E. Thormann, ACS Appl. Mater. Interfaces 4 (2012) 5534–5541.
[31] J.E. Sader, J.W.M. Chon, P. Mulvaney, Rev. Sci. Instrum. 70 (1999) 3967–3969.
[32] B. Quignon, G.A. Pilkington, E. Thormann, P.M. Claesson, M.N. Ashfold, D. Mattia, H. Leese, S.A. Davis, W.H. Briscoe, Acs Nano 7 (2013) 10850–10862.
[33] G.A. Pilkington, E. Thormann, P.M. Claesson, G.M. Fuge, O.J. Fox, M.N. Ashfold, H. Leese, D. Mattia, W.H. Briscoe, Phys. Chem. Chem. Phys. 13 (2011) 9318–9326.
[34] P.M. Hansson, P.M. Claesson, A. Swerin, W.H. Briscoe, J. Schoelkopf, P.A.C. Gane, E. Thormann, Phys. Chem. Chem. Phys. 15 (2013) 17893–17902.
[35] M. Rodahl, F. Höök, A. Krozer, P. Brzezinski, B. Kasemo, Rev. Sci. Instrum. 66 (1995) 3924–3930.
[36] G. Sauerbrey, Zeitschrift für physik 155 (1959) 206–222.
[37] D. Johannsmann, K. Mathauer, G. Wegner, W. Knoll, Phys. Rev. B 46 (1992) 7808–7815.
[38] M. Rodahl, B. Kasemo, Sens. Actuators, A 54 (1996) 448–456.
[39] U. Seifert, R. Lipowsky, Phys. Rev. A 42 (1990) 4768–4771.
[40] W. Helfrich, Z. Naturforsch C 28 (1973) 693–703.
[41] H. Bermúdez, D.A. Hammer, D.E. Discher, Langmuir 20 (2004) 540–543.
[42] U. Seifert, R. Lipowsky, in Handbook of Biological Physics, R. Lipowsky and E. Sackmann (eds.), North-Holland, 1995, 1, 403–463.
[43] G. Cevc, W. Fenzl, L. Sigl, Science 249 (1990) 1161–1163.
[44] R. Lipowsky, U. Seifert, Mol. Cryst. Liq. Cryst. 202 (1991) 17–25.
[45] R. Lipowsky, Nature 349 (1991) 475–481.
[46] G. Battaglia, C. LoPresti, M. Massignani, N.J. Warren, J. Madsen, S. Forster, C. Vasilev, J.K. Hobbs, S.P. Armes, S. Chirasatitsin, A.J. Engler, Small 7 (2011) 2010–2015.
[47] K. Kawakami, Y. Nishihara, K. Hirano, J. Phys. Chem. B 105 (2001) 2374–2385.
[48] U. Raviv, J. Klein, Science 297 (2002) 1540–1543.
[49] R. Goldberg, J. Klein, Chem. Phys. Lipids 165 (2012) 374–381.
[50] R. Sorkin, N. Kampf, Y. Dror, E. Shimoni, J. Klein, Biomaterials 34 (2013) 5465–5475.
[51] M. Chen, W.H. Briscoe, S.P. Armes, J. Klein, Science 323 (2009) 1698–1701.
[52] X. Liu, E. Thormann, A. Dedinaite, M. Rutland, C. Visnevskij, R. Makuska, P.M. Claesson, Soft Matter 9 (2013) 5361–5371.
[53] M. Müller, S. Lee, H.A. Spikes, N.D. Spencer, Tribol. Lett. 15 (2003) 395–405.
[54] W.H. Briscoe, S. Titmuss, F. Tiberg, R.K. Thomas, D.J. McGillivray, J. Klein, Nature 444 (2006) 191–194.
[55] W.H. Briscoe, F. Speranza, P.X. Li, O. Konovalov, L. Bouchenoire, J. van Stam, J. Klein, R.M.J. Jacobs, R.K. Thomas, Soft Matter 8 (2012) 5055–5068.
[56] F. Speranza, G.A. Pilkington, T.G. Dane, P.T. Cresswell, P.X. Li, R.M.J. Jacobs, T. Arnold, L. Bouchenoire, R.K. Thomas, W.H. Briscoe, Soft Matter 9 (2013) 7028–7041.
[57] W.H. Briscoe, M. Chen, I.E. Dunlop, J. Klein, J. Penfold, R.M.J. Jacobs, J. Colloid Interface Sci. 306 (2007) 459–463.
[58] B. Sironi, T. Snow, C. Redeker, A. Slastanova, O. Bikondoa, T. Arnold, J. Klein, W. H. Briscoe, Soft Matter 12 (2016) 3877–3887.